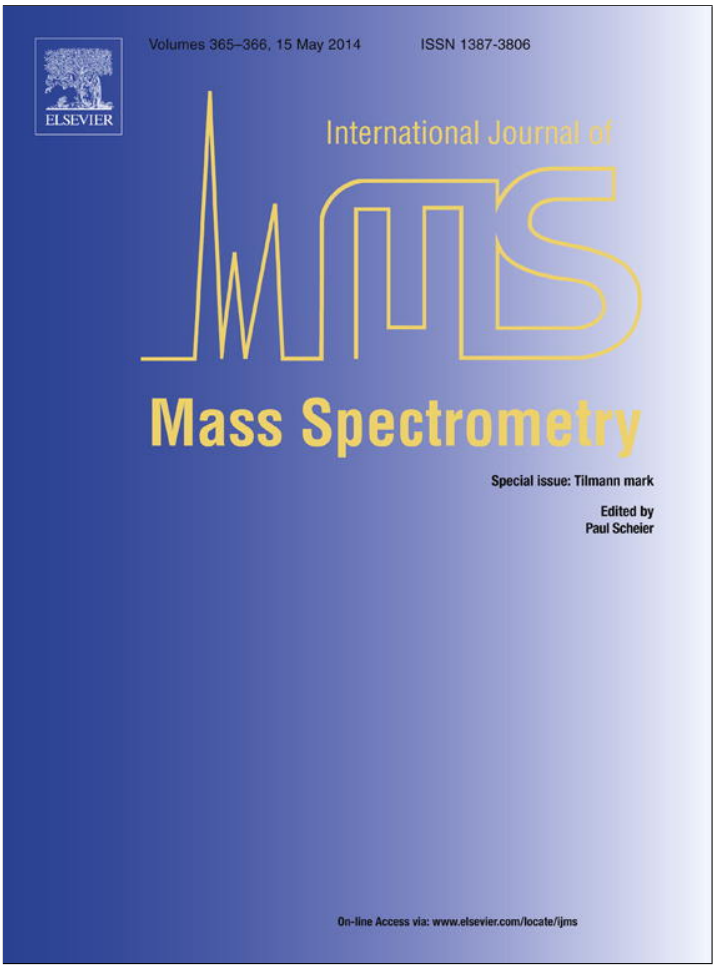

International Journal of Mass Spectrometry 365–366 (2014) 377–383

Contents lists available at ScienceDirect

International Journal of Mass Spectrometry

journal homepage: www.elsevier.com/locate/ijms

Attaching electrons to a 3-ring acene: Structures and dynamics of anions in gas-phase anthracene

Fabio Carelli[a,b], Franco Antonio Gianturco[a,c,*], Mauro Satta[b], Francesco Sebastianelli[b]

[a] Institute of Ion Physics, Innsbruck University, Technikerstrasse 25, 6020 Innsbruck, Austria
[b] Department of Chemistry, The University of Rome 'Sapienza', P.le Aldo Moro 5, 00185 Rome, Italy
[c] Scuola Normale Superiore, Piazza de' Cavalieri, 50125 Pisa, Italy

ARTICLE INFO

Article history:
Received 25 November 2013
Received in revised form 13 March 2014
Accepted 13 March 2014
Available online 10 May 2014

This work is affectionately dedicated to Prof. Dr. Tilmann Maerck, a good friend and a great scientist.

ABSTRACT

The existence of metastable anions, formed in the gas-phase by electron scattering off anthracene molecules is investigated via both quantum dynamics calculations and quantum chemical structure calculations. The differences in the sign of the experimentally known electron affinity (EA), positive small for anthracene, and of its values obtained from different methods employed to estimate it in the present work, are shown to be related to level of computations and to the increasing effects from electron–electron dynamical correlation (as well as the all-important bound-continuum exchange) which act to selectively stabilize the attaching electron in this three-ring acene, the first of these polycyclic aromatic hydrocarbons (PAHs) to exhibit stable anions in the gas phase.

1. Introduction

In the early 1970s, the first spectra of some of the brightest infrared sources in the interstellar and circumstellar spaces revealed the unexpected presence of strong emission features from 3.3 to 8.6 μm (e.g.: see [1]) and references given therein). Since then, several types of observations have shown that these features dominate the spectra of almost all objects, including the H II regions, the reflection nebulae, the young stellar objects, the post-AGB objects and the general interstellar medium (ISM) of the Milky Way and of other galaxies (e.g. see Ref. [2] as an example). It is now well established that these IR emission features are due to the vibrational relaxation of UV-pumped polycyclic aromatic hydrocarbons molecules (PAHs) with sizes ranging from 20 to 100 carbon atoms [3]. Furthermore, rapid advances in computational power and experimental resolution have allowed to suggest in the forest of diffuse, unidentified infrared bands (DIBs) the presence of radicals, charged cationic and anionic species as the IR emitters of choice [4–6].

It is therefore of great current interest to be able to understand, at the molecular level, the sequence of processes which can lead to photoionization or to chemical charge exchange on such systems, as well as to the formation of stable and metastable anions by interactions with the environmental electrons [7].

The possible role of free electrons generated by photoionization of the most abundant species of the ISM (H, D, He) has been discussed many times in the literature over the years [8,9] and our group has analyzed in some detail the end-line of such processes when applied to aromatic species like coronene [10], benzene [11], and phenyl [12], where in fact the possible role of transient negative ions (TNIs) in the continuum has been shown to be linked to the stabilization of anionic species with significant sizes of attachment rates [13]. Such possibilities are particularly intriguing for the anthracene molecule since its capability of forming stable anionic species sits at the positive side of the energy range with respect to its smaller predecessors in the series: benzene and naphthalene have, in fact, negative EA values [14]; while, the anthracene's EA is shown by experiments to be rather small and positive: $+0.530 \pm 0.005$ eV [15,16]. Hence, while the smaller acenes are expected to only have metastable anions, which then decay either by autodetachment or by dissociative electron attachment (DEA) driven by more complicated fragmentations [14], anthracene only forms barely bound anions after the metastable attachment of near-threshold electrons [17].

Additionally, recent high-level computational studies of condensed rings aromatic acenes [18,19] have pointed out that, from the analysis of the composition of their multiconfigurational wavefunctions, the topologies of the natural orbitals in symmetry-unrestricted CASSCF calculations indicate that such systems exhibit a ^1A_g closed-shell electronic ground state and, at the same time,

* Corresponding author at: Institute of Ion Physics, Innsbruck University, Technikerstrasse 25, 6020 Innsbruck, Austria.
E-mail address: Francesco.Gianturco@uibk.ac.at (F.A. Gianturco).

http://dx.doi.org/10.1016/j.ijms.2014.03.014
1387-3806/

indicate the diradical and polyradical character of the acenes with more polycondensed aromatic rings. In other words, the highest occupied molecular orbitals require increasingly smaller amounts of energy for the singlet–triplet gap as the acenes get bigger in size, thus causing single occupancy of both the highest occupied natural orbital (HONO) and the lowest unoccupied natural orbital (LUNO). This diradical character therefore changes the correlation contributions as the anion is being formed, i.e. the corresponding extra-electron will become, or will not manage to become, a bound electron in the stable anion depending on the extent of the correlation effects included in the calculations. The previous discussion therefore points at the computational difficulties which exist for the realistic evaluation of the structural features of the bound anions of anthracene as well as for the reliable assessment of the dynamics for electron attachment rates to this system, i.e. on the effective role that the formation of resonant, metastable anions plays on controlling the final efficiency of low-temperature attachment rates to PAHs, a feature of importance for their modelling in dark clouds and in circumstellar envelopes [13].

The present study therefore intends to revisit our earlier study on the anthracene metastable anions [17] by employing increasingly more sophisticated treatments of correlation forces in both quantum chemistry studies and scattering calculations. In the latter instance we shall also improve on the treatment of bound-continuum exchange interactions. We shall therefore analyse in some detail the possible existence of metastable anions for anthracene as well as the actual structures of a bound anion in its ground electronic state. The structural features of the electronically excited anionic configurations will be also linked with the resonant anionic complexes obtained from quantum scattering calculations in the low-energy range.

The following section will briefly describe the cross-section quantum calculations. We shall employ a multichannel scattering approach used by us many times before so that only a brief outline of the method will be given, together with relevant references where further details could be obtained. We shall also report here the details of the new and varied structure calculations employed for the analysis of its anions.

Section 3 shall give our results from all calculations and compare our findings from both the dynamics and structure studies, while Section 4 will summarize our conclusions.

2. Computational methods

2.1. An outline of the scattering calculations

Since the quantum dynamical equations used for this study have been described in detail many times before [20,21], we only present here a brief outline of it and refer the reader interested in more details to those publications.

The total $(N+1)$-electron wave function is constructed as an antisymmetrized product of one-electron wave functions obtained from Hartree-Fock orbitals of the neutral ground state molecular target, considering the N bound electrons in their ground-state configuration during the whole scattering process: thus, no core-excited resonances are allowed in our modelling. Each of the three dimensional wave functions describing a given electron is then expanded around the molecular center of mass (Single Center Expansion, SCE) so that for each of the bound molecular electrons we have

$$\phi_i^{p\mu}(r,\hat{\mathbf{r}}|\mathbf{R}) = \sum_{\ell h} \frac{1}{r} u_{\ell h,i}^{p\mu}(r|\mathbf{R}) \chi_{\ell h}^{p\mu}(\hat{\mathbf{r}}) \tag{1}$$

and for the scattered particle

$$\psi^{p\mu}(r,\hat{\mathbf{r}}|\mathbf{R}) = \sum_{\ell h} \frac{1}{r} f_{\ell h}^{p\mu}(r|\mathbf{R}) \chi_{\ell h}^{p\mu}(\hat{\mathbf{r}}) \tag{2}$$

In the above SCE representations, the superscripts label the μth irreducible representation of the pth symmetry group to which the molecule belongs at the fixed nuclear geometry $\mathbf{R}$, and the subscripts refer to each of the angular channels under considerations; the radial coefficients $u_{\ell h}^{p\mu,\alpha}$ for the bound molecular electrons are numerically evaluated by a quadrature on a radial grid [22]. The angular functions $X_{\ell h}^{p\mu}$ are given as

$$\chi_{\ell h}^{p\mu}(\hat{\mathbf{r}}) = \sum_m b_{\ell m h}^{p\mu} Y_{\ell m}(\hat{\mathbf{r}}). \tag{3}$$

where the coefficients $b_{\ell m h}^{p\mu}$ are described and tabulated in Ref. [23]. The ensuing coupled partial integro-differential quantum scattering equations evaluate the unknown radial coefficients $f_{\ell h}^{p\mu}$ for the (N+1)th continuum electron:

$$\left[\frac{d^2}{d^2r} - \frac{\ell(\ell+1)}{r^2} + 2(E-\epsilon)\right] f_{\ell h}^{p\mu}(r|\mathbf{R}) = 2\sum_{\ell' h'} \int dr' V_{\ell h,\ell' h'}^{p\mu}(r,r'|\mathbf{R}) f_{\ell' h'}^{p'\mu'}(r'|\mathbf{R}) \tag{4}$$

where E is the collision energy and ϵ is the electronic eigenvalue for the ground state energy so that $k^2/2 = E-\epsilon$, k being the asymptotic momentum of the elastically scattered electron.

For a target which has a closed shell electronic structure, with $n_{occ} = N/2$ doubly occupied molecular orbitals, the static-exchange (SE) potential has the following form:

$$V_{SE} = \sum_{\gamma=1}^{M} \frac{Z_\gamma}{|\mathbf{r}-\mathbf{R}_\gamma|} + \sum_{i=1}^{n_{occ}} \left(2\hat{J}_i - \hat{K}_i\right) = V_{st} - \sum_{i=1}^{n_{occ}} \hat{K}_i \tag{5}$$

where $\hat{J}_i$ and $\hat{K}_i$ are the usual static potential and the non-local exchange potential operator, respectively. We further model the correlation and polarization effects via the following optical potential:

$$V_{cp} = V_{Corr}(r), \quad r \le r_{match} \tag{6}$$

$$V_{cp} = V_{Pol}(r), \quad r > r_{match} \tag{7}$$

employing density related models which have been described before for the short-range correlation effects [20,21]. We then generate the exchange interaction with the Free-Electron-Gas-Exchange model proposed by Hara (HFEGE [24]), V_{HFEGE}:

$$V_{HFEGE}(\mathbf{r}|\mathbf{R}) = -\frac{2}{\pi} K_F(\mathbf{r}|\mathbf{R}) \left[\frac{1}{2} + \frac{1-\eta^2}{4\eta} \ln\left(\frac{1+\eta}{1-\eta}\right)\right]. \tag{8}$$

When dealing with closed-shell systems as the present case, the electronic density $\rho(\mathbf{r}|\mathbf{R})$ is given as

$$\rho(\mathbf{r}|\mathbf{R}) = \int |\det||\phi_1(\mathbf{r}_1)\phi_2(\mathbf{r}_2)\ldots\phi_{n_e}(\mathbf{x}_{n_e})|||^2 \; d\mathbf{x}_2 \; d\mathbf{x}_3 \ldots d\mathbf{x}_{n_e} \tag{9}$$

is evaluated by assigning 2 as the occupation number of each of doubly occupied MOs in the neutral targets of the present study. In other words, the scattered electron initially interacts with the neutral molecular targets at the fixed geometry of their equilibrium structures. This final potential provides the so-called static-model-exchange-correlation-polarization (SMECP) potential accounting for the interaction forces between the impinging free electron and

the target molecule. The coupled set of integrodifferential equations now takes the form:

$$\left[\frac{d^2}{d^2r} - \frac{\ell(\ell+1)}{r^2} + 2(E-\epsilon)\right] f_{\ell h}^{p\mu}(r|\mathbf{R}) = 2\sum_{\ell' h'} V_{\ell h,\ell' h'}^{p\mu}(r) f_{\ell h}^{p\mu}(r), \quad (10)$$

where the potential coupling elements are

$$V_{\ell' h',\ell h}^{p\mu} = \langle X_{\ell' h'}^{p\mu}(\hat{r})|V(\mathbf{r})|X_{\ell h}^{p\mu}\rangle = \int d\hat{r} X_{\ell' h'}^{p\mu} V(\mathbf{r}) X_{\ell h}^{p\mu} \quad (11)$$

The numerical solutions of the coupled equations produce the relevant *K*-matrix elements which will in turn yield the final integral cross sections [22].

2.2. The quantum chemistry structural calculations

Given the crucial role played by the correct inclusion of correlation effects in the calculations of EA in the title system, as already discussed in Ref. [7], it is interesting to remind readers of the different aspects of the problem which have been already addressed in the existing literature and which could contribute in generating uncorrect estimates of the final electron affinities in anthracene (ANTH):

(i) the incipient diradical nature of the HONO and LUNO, as discussed in [18,19] in the ANTH system, could lead to the need for a more realistic inclusion of correlation effects between the impinging free electron and either of the delocalized natural orbitals mentioned above. Hence the model we have described in the previous section to include bound-free correlation forces may not be realistic enough for the special nature of a condensed-ring target like ANTH;
(ii) the large effects played by the vibrational energy content of such system during the experimental measurement of EA values has been already discussed in earlier calculations [7] where it was found that the simple inclusion of zero point vibrational energy (ZPVE) corrections changed the vertical attachment energies by more than 100 meV. This means that the search for small EA values as those present in the ANTH could be greatly affected by the methods employed to include such a correction in both structural and scattering calculations;
(iii) since resonant compound states (TNI states) can be described as excited electronic states of the corresponding molecular anions, one should be very carefully employing very large basis set expansions when searching for them in structural calculations of such states.

We shall try to address all of the above problems by calculating anion states of ANTH, at the equilibrium geometry, and using a broad range of basis set expansions. We employed such large basis set within an Unrestricted Hartree Fock (UHF) approach, followed by the use of Density functional (DFT) methods that traditionally allow for a more correlated description of the anionic state associated with the ground electronic configuration [25]. We also used the Configuration Interaction treatment including all single excitations (CI(S)) to look at both ground electronic states and excited virtual states of the anionic configurations for the present system [25]. Although the latter method is essentially keeping the correlation effects at the Hartree-Fock level, it however allows us to generate a spatial description of the excited electronic states from the large basis sets we are employing, so that we compare them with the results from our scattering calculations.

3. Results and discussion

3.1. The electron affinity of anthracene

As mentioned in the introduction, the three-ring acene has been found to have an EA value which is small and positive, i.e. the physically stable anion, $ANTH^-$, is lower in energy than its corresponding neutral, ANTH, both when the same geometry is kept for the anion (vertical EA) and when the final anion geometry is separately optimized (adiabatic EA). Since the one-ring system (benzene) turns out to have a *negative* EA which is quite large (∼−1.12 eV [14]), and the two ring system (naphthalene) also produces a metastable anion with a smaller and negative EA (∼−0.19 eV [14]), it is reasonable to deduce that the addition of the third, condensed aromatic ring manages to stabilize the anion thanks to the progressive increase along the series of electron-electron short-range dynamical correlation effects: the next four-ring system (tetracene) has, in fact, a yet larger and positive EA value of ∼1.04 eV [14].

To follow such an effect as displayed by quantum chemical calculations, we have carried out an extensive series of total energy calculations, without ZPVE correction for the moment, for both the neutral molecule at its equilibrium geometry and the corresponding ground-state anion at the same geometry (vertical EA) or at its optimized geometry (adiabatic EA).

To control the effect of polarization forces, we have employed both ROHF and UHF calculations with different basis sets, as well as performed CI calculations and DFT estimates, the last two approaches intended to include increasingly larger contributions from correlation forces.

The results are reported by Table 1.

Several, interesting points can be noted from the above calculations:

(i) the simplest Hartree-Fock (HF) calculation provides an unstable anionic state with the largest energy gap; given the actual experimental value of the EA for ANTH, we see here an error of about 1.53 eV. The lack of correlation correction clearly prevents the delocalized aromatic electrons of the π-system to adjust correctly to the extra-electron, thereby not binding it to the target as it occurs instead experimentally [15];
(ii) all the different choices of basis sets within the Unrestricted HF approach fail to correctly bind the anion, although the error in the EA estimates (see Table 1) is now being reduced to about 1.0 eV. The target correlation effects are slightly improved, but not enough to stabilize the final ($ANTH^-$) species;
(iii) the partial inclusion of correlation forces using the MP2 approach improves the stabilization of the anion, so that the EA value, although still negative, is very close to zero in such a way that, for the larger basis set choice, only less that 0.5 eV still need to be recovered;

Table 1
Computed and measured EA for anthracene. The EA experimental value of the latter is 0.530 ± 0.005 eV, see Ref. [15].

Method/expansion basis set	$EA_{vertical}$ (eV)	$EA_{adiabatic}$ (eV)	$\epsilon_{B_{3u}}$
HF/cc-pVTZ	−0.90	–	+2.070
UHF/cc-pVTZ	−0.58	−0.44	−0.275
UHF/aug-cc-pVTZ	−0.47	–	−0.387
UHF/cc-pVQZ	−0.54	–	−0.340
UHF/cc-pV5Z	−0.17	–	−0.380
CI(S)/cc-pVTZ	−0.58	−0.44	−0.275
MP2/cc-pVTZ	−0.04	−0.01	–
MP2/cc-pVQZ	−0.09	–	–
DFT(UB3LYP)/cc-pVTZ	+0.42	+0.50	+1.140
DFT(UB3LYP)/aug-cc-pVTZ	+0.53	–	+0.924

(iv) the additional inclusion of more correlation effects at the DFT level, albeit done with a basis set expansion at the triple-zeta level, is seen to provide the EA value very close to experiments (∼0.53 eV [15]) once the adiabatic corrections are included;
(v) additional basis set expansion choices, which are all shown in our table, also indicate that the evaluation of the EA in this special molecule is describing a bound anion configuration where the extra electron is fairly compactly distributed around the nuclear network of the molecular equilibrium geometry, as we shall discuss below in more details. Hence, additional diffuse functions modify only in part the general physical picture provided by the more compact basis set expansions reported in that table;
(vi) it is also interesting to note that the eigenvalues of the SOMO describing the anionic electron become negative as soon as one goes beyond the restricted HF treatment, thus indicating that the b_{3u} additional orbital is striving to describe a bound electron in the anion and not a metastable one. However, the actual EA value for the full system only becomes correctly positive when the additional dynamical correlation between residual electrons in the whole anthracene molecule is more realistically described, as also discussed above. For the DFT calculations the use of a more correlated $(n+1)$ electron system provides the best agreement for the EA value, although the corresponding SOMO now maintains a positive eigenvalue, to confirm the rather approximate physical meaning of such quantity with respect to the more correct energy difference as estimate of the EA value.

One therefore can say that the crucial element in the interaction forces between the extra electron and the aromatic system of ANTH is given by the correct inclusion, as much as possible, of electron–electron dynamical correlation effects, as well as the correct exchange interaction between the $(N+1)$ electrons. Such considerations, therefore, can be further analyzed when looking at the dynamics of electron scattering from ANTH targets, as discussed below.

3.2. Anion formations via electron scattering calculations

The structural calculations discussed in the above pages indicate that all the calculations for the ground state of $ANTH^-$ have as the lowest electronic configurations one with a b_{3u} molecular orbital (MO) as the SOMO (singly occupied MO). However, all calculations but the DFT results also indicate that the insufficient contributions from correlation effects in all the examples of tables I and II, still with the exclusion of the DFT calculations, produce metastable anionic state with respect to the neutral species. It is therefore of interest to see what are the outcomes of the dynamical evolution of metastable ions when they are directly produced by low-energy electron scattering processes. We shall do it by following the computational model outlined in Section 2.

Earlier calculations carried out by us on this system [17], have indicated that the $^2B_{3u}$ state of the anion was a metastable state located about 1.16 eV above the neutral: this result was achieved at the level of electron–electron correlation contributions described within our electron–density functional form [20], also extensively tested by us in smaller molecules (e.g. benzene) in earlier work [26]. If the DFT structure calculations are correct, then the effects of correlation forces on the scattering cross sections need to be carefully analyzed for this special class of acenes, for the reasons briefly mentioned in the Introduction.

We have therefore carried out a new set of scattering calculations for metastable anions of $(ANTH)^-$, revisiting the results already presented in [17] and employing different types of models for dynamical electron–electron correlation potentials and for exchange interactions between the continuum and the bound electrons. In particular, the additional tests which we carried out within the treatment of the continuum-bound electron–electron dynamical correlation effects in the present multichannel quantum scattering calculations involve the following changes:

(i) orthogonality constraints. Since the scattered electron wavefunction is not exactly describing a virtual state from the target HF molecular orbitals (given the marked effects caused by the added scattering correlation-polarization parts of the interaction) it is not an eigenfunction of the Hamiltonian for the target molecular electrons. Hence, one must make sure that it remains orthogonal to the bound orbitals of the same symmetry [21]. For polyatomic targets like the ANTH molecule such constraint is usually satisfied since the strength of the static and exchange contributions dominates. However, when enforcing this orthogonality, one makes sure that the nodal structure of the scattered electron remains the correct one also in the outer regions of the target density and therefore allows for an increase of overall attractive effects from the target nuclei [21];
(ii) using a different short-range correlation potential. In the treatment of the resonances for ANTH, reported by Ref. [17], we have employed the form described in Ref. [20] and obtained earlier by Perdew and Zunger (PZ [27]). A stronger, more attractive density functional form for the short-range correlation had been suggested by Padial and Norcross (PN [28]) for diatomic targets and further implemented by us for polyatomic molecules [29]. The latter potential was employed by us for several systems of medium-size targets (e.g., see Ref. [26]) and yielded interesting results in terms of good agreement with existing experiments (for a recent comparison also see Ref. [30]). Once the PN correlation model was employed in connection with the constraints of (i), the $^2B_{3u}$ resonance moves even more strongly towards threshold, as clearly shown in Fig. 1, where both the orthogonalization constraint and either of the V_{cp} potentials was employed.

In order to see even more in detail the effect of changing the strength of bound-continuum, electron–electron interaction, we further report in Fig. 1 what happens to the lowest resonance generated by our scattering calculations, the metastable anion of $^2B_{3u}$ symmetry, when the condensed ring geometry is modified by lengthening the C–C distances in all of them: the target bound electron densities are recomputed each time, thereby adjusting them to their less efficient screening of the attractive nuclear charges.

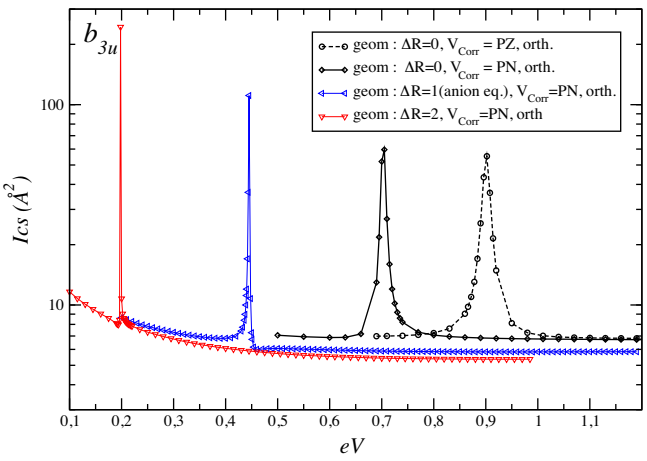

Fig. 1. Evolution of the b^*_{3u} resonance in anthracene as a function of different ring size and potential strength modifications. See text for further details.

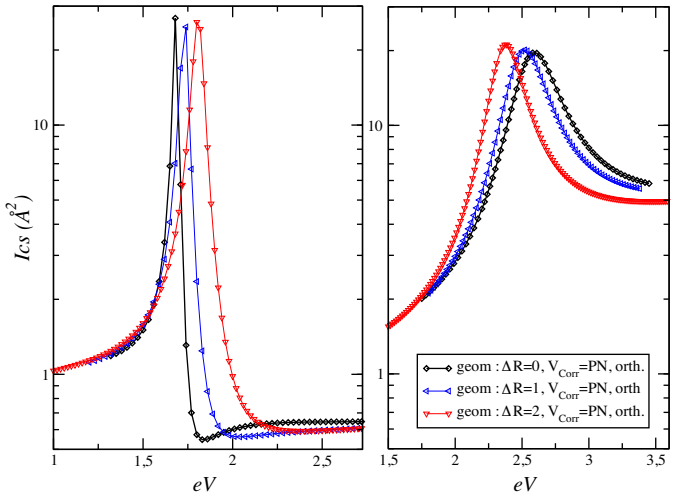

Fig. 2. Effect of geometry changes on the locations and shapes for the ^2A_u resonance (left panel) and the $^2B_{1g}$ resonance (right panel). See main text for further details.

As a consequence, we therefore increase the static interactions between the nuclei and the extra electron and further stabilize the resonance.

The data in Fig. 1 refer to two additional geometries for (ANTH$^-$) ground state: the $\Delta R = 1$, which correspond to the stretched geometry of the anion as suggested in Ref. [31], and the $\Delta R = 2$, which corresponds to doubling the previous bond stretches. Both cases amount to geometry changes of no more than 5%. The calculations clearly show how dramatically the resonance's location moves down on the energy scale, essentially aiming at making the SOMO given by the scattering calculations much closer to a bound state with respect to the neutral molecule (positive EA value).

The effects of such geometry changes are also given in the two panels of Fig. 2 for the next two resonances of ANTH$^-$ corresponding to two different excited electronic configurations of this system: the ^2A_u and the $^2B_{1g}$ resonances discussed in [17,30]. We have therefore repeated the same set of modified calculations for both resonances: the results and in particular the effects associated to the geometry changes are given by the two panels of Fig. 2.

In this example, we show the calculations only for the correlation potential given via the DFT modeling of Ref. [28], since we have already seen from Fig. 1 that the PZ potential would have similar effects.

The two panels indicate that the use of geometry changes to increase the scattered electron interaction with the target does not have, for the next two higher resonances, the same dramatic effects as the one seen for the $^2B_{3u}$ 'resonance' that essentially moved to become a bound state. In fact, both resonances remain of the same widths and nearly at the same positions as those shown by the calculations at the equilibrium geometry of ANTH. This means that their spatial shapes, that we shall further analyse later, are much less sensitive to both changes of nuclear geometries and of the correlation potentials.

In conclusion, we see that it is principally the lowest SOMO configuration of (ANTH$^-$), the $^2B_{3u}$ state of the anion, which is most strongly affected, depending on the accuracy with which the attractive correlation effects are included within the total interaction between the target molecule and the impinging electron. In fact, the $^2B_{3u}$ is the only anion that is produced as a bound anion by the DFT quantum chemistry calculation of Table 1, and that is also the very anionic state which is seen to move into the bound state region when our scattering calculations are made to employ an interaction model which provides stronger, more attractive, correlation forces.

Furthermore, the use of stronger correlation forces and the deformation of the rings towards the anionic structure and beyond for the ANTH molecule, as reported in Fig. 1, indicates that the lowest metastable state of (ANTH$^-$), the $^2B_{3u}$ anionic configuration, can move towards the ground electronic state of a bound negative ion (with positive, albeit still small EA value) provided the correlation dynamics between the scattered electron and the bound electrons of the target is treated with great care and made as strong as possible within the chosen models.

In order to further explore the effects on the scattering calculations of additional changes in the interaction forces, we note now that the use of the local exchange interaction described in the previous Section was found to be less attractive than the true non-local exchange potential even in much simpler diatomics [32] a long time ago. We had already developed earlier on a much more computationally expensive alternative to evaluate exchange, one based on the Schwinger variational expression of the scattering matrix [33,34] that further included Pade' approximants corrections. Briefly, the iterative treatment of the exchange interaction consists in dividing the interaction into two parts: an approximate, local potential V_L that includes an initially simplified, semiclassical exchange form (SME [17]), plus a difference potential V_D which adds the correction due to using exact exchange interaction. The latter is initially defined as $V_{HFEGE} - V_{SME}$ to start the iterative process. The solution to a purely local problem via the potential $V_T = V_L + V_D$ could be written as:

$$H_L\phi_L = E\phi_L \tag{12}$$

where $H_L = -1/2\,\nabla^2 + V_L$ and the associated Green's function is defined as

$$(E - H_L)G_L = 1. \tag{13}$$

Any element of the final scattering matrix K for the full potential V_T can be written as

$$K_{pq}^{(T)} = K_{pq}^{(L)} + K_{pq}^{(D)} \tag{14}$$

where the correction terms is

$$K_{pq}^{(D)} = -2\langle\phi_L|V_D|\phi_L\rangle \tag{15}$$

which can also be written via a Born series expansion [17]

$$K_{pq}^{(D)} = -2\sum_{j=0}^{\infty}\langle\phi_p|V_D(G_LV_D)^j|\phi_q\rangle. \tag{16}$$

The convergence of this sum turns out to be greatly enhanced by using Pade' approximants [33] of [N/N] order, thereby allowing the calculations to incrementally modify the potential by using increasingly more accurate forms of the Green's function G_L in Eq. (16) [17,34].

The present results on the lowest three resonant anionic configurations of (ANTH$^-$) are shown by Fig. 3, where the three panels report the final locations of the resonant peaks for the three cross section components already discussed in Figs. 1 and 2.

One clearly sees now that the incremental strengthening of the dynamical correlation forces (via the PN potential form) and of the bound-continuum exchange interaction (via the iterative Schwinger procedure) has a dramatic effect on the lowest metastable state $^2B_{3u}$: the resonance has now moved out of the positive energy range and becomes a bound state, namely the stable molecular anion discussed before. Furthermore, the next higher resonances have also moved down on the energy scale from their original positions, the latter marked by the dashed vertical lines. Thus, the ^2A_u metastable anion is now about at 0.80 eV and the $^2B_{1g}$ resonance has also moved down to about 1.90 eV. It is interesting to note that they have kept their original widths and are now fairly close to the recent model calculations discussed in Ref. [30]. Their

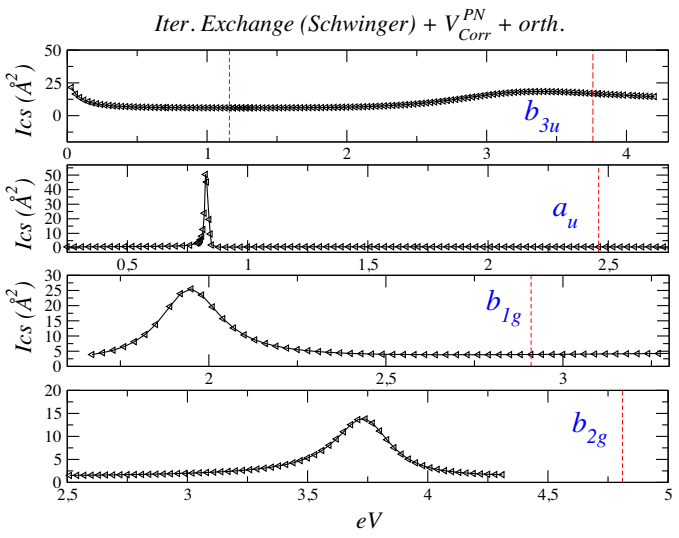

Fig. 3. Computed locations and widths of the lowest three resonant anionic states of anthracene. See main text for further details.

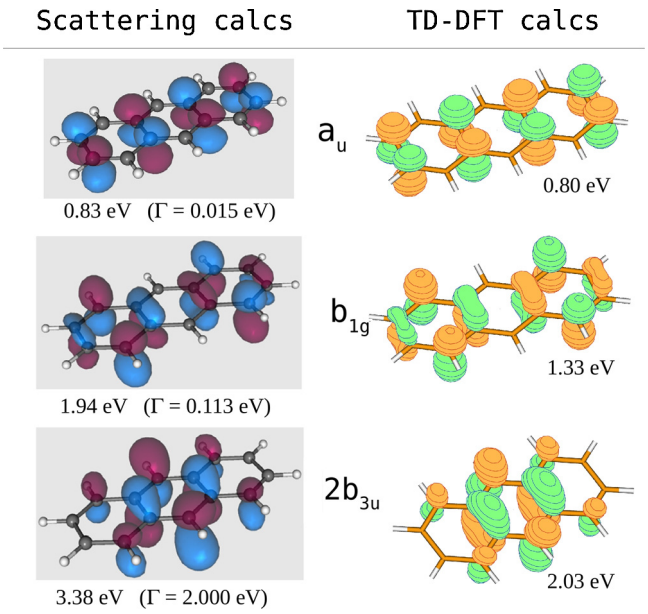

Fig. 5. Computed spatial structures of the excited anionic states of the anthracene molecule. Left panels: the SOMO wavefunctions, from scattering calculations; right panels: the SOMO wavefunctions from quantum chemicalstructure calculations. See main text for further details.

calculations show the ^2A_u resonance to be at 0.714 eV with a width of 7 meV, to be compared with our 0.78 eV and 10 meV of Fig. 3. Additionally, the $^2B_{1g}$ resonance was found in [30] to be at about 1.1 eV with a width of 60 meV: here we find it at about 1.90 eV and with a width of more than 600 meV, closer to our earlier results of [17], thus indicating the presence of probably excessively stronger attractive effects implicit in the quantum chemistry model of [30]. The lowest two experimental resonances, were found to have a centroid of locations [14] at 0.7 eV and 1.3 eV but no width information have been given.

3.3. The spatial shapes of metastable electron

Another interesting comparison between the outcomes of the scattering calculations and those from the quantum chemical studies which we have presented so far is that of comparing the spatial structures of the anion's excess electron produced by the two approaches. An earlier study on single-ring acenes [12] had shown that both resonant and bound extra-electrons where described in very good agreement by either approach, so it is of interest to extend the study to the present acenes.

The data in Fig. 4 report the lowest $^2B_{3u}$ SOMO produced by the scattering calculations (left panel), the CI(S) calculations (central panel) and the anion's ground state from the DFT calculations (right panel).

The sequential presentation of the three different wavefunctions follows the relative stability of the computed ground state of the anthracene anion: the left panel describes a metastable SOMO located, as seen in Fig. 1, at about 0.7 eV above the neutral when the (V_{cp}^{PN} + orth.) is employed, while the central panel presents the same metastable SOMO from CI(S) calculations, which is 0.58 eV above the neutral (see Table 1). On the other hand, the panel on the right reports the b_{3u} SOMO from DFT quantum chemistry calculations which now describes a bound anion about 0.44 eV below the neutral. All three orbitals are clearly seen to be essentially identical, indicating that in all cases the calculations produce the anionic lowest configuration to be a $^2B_{3u}$ state which, however, moves from metastability to a bound state depending on the level of bound-continuum electron–electron dynamical correlation introduced in the calculations.

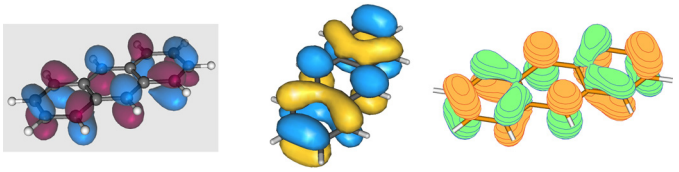

Fig. 4. Spatial shapes of the resonant and bound wavefunctions associated with the b_{3u} SOMO of the anthracene anion. Left panel: scattering resonant orbital; central panel: metastable orbital from the CI(S) calculations; right panel: bound orbital from the DFT calculations.

A further computational example of the symmetry control on the features of the anionic states, this time applied to the excited, metastable anions, could be seen from the data reported by Fig. 5, where we now compare the next three resonant anionic states as obtained from the present scattering calculations with the virtual anionic states identified via the quantum chemical calculations. The latter method, in fact, is able to improve on the correlation forces included by the simpler HF calculations, thus behaving similarly to the scattering calculations where correlation effects are included via the PN or PZ modeling reported in the previous section.

The following comments could be gathered from an analysis of the excess electron maps reported in that figure:

(i) the energy sequence of the three metastable anionic states turns out to be similar from both calculations since they all fall within a range of about 3.0–4.0 eV;
(ii) their spatial structures are also remarkably similar, indicating that both sets of calculations, albeit very different, produce the same symmetry-controlled sequence of metastable, excited anions.

From the last two figures, therefore, we can see that the present calculations provide a realistic description of the anionic states of ANTH, both for its ground and the excited states. In the case of the former, however, we clearly see in Fig. 4 that the inclusion of greater contributions from the short-range electron–electron dynamical correlation plays a crucial role in producing the correct bound state for the anion, although no changes in the spatial shape of this extra-electron are found.

4. Present conclusions

In this paper we have tackled the problem of producing from accurate calculations a realistic description of the behaviour of an aromatic molecule, the three-ring acene anthracene in the gas-phase process of forming both stable and metastable anionic complexes when interacting with free electrons.

The process is certainly relevant for producing a theoretical confirmation of the earlier experimental findings on several acenes [14,15], besides being of direct interest for the analysis of negative ion formation in PAHs [2]. Additionally, the existence for anthracene of a very small and positive EA value, the first of the acenes to show this effect [7], produces an arrangement with particular computational interest since the final production of a stable (bound) anion of ANTH is delicately linked to the correct inclusion of dynamical correlation and of bound-continuum exchange interactions in all types of calculations.

The results we have reported in the previous section where carried out by using first quantum chemistry analysis of the anionic electronic states and then a quantum scattering modelling of the attachment process. The use of a wide variety of basis set expansions for the quantum chemistry data, and of different forms of bound-continuum interactions for the scattering calculations, is shown to produce essentially the same trend in the various calculations and basically the same information on the ($ANTH^-$) in its ground and in a few of its excited electronic states. More specifically:

(i) the $^2B_{3u}$ anthracene anion is shown to be a stable configuration which yields a bound anion with respect to its neutral counterpart: the vertical EA, without VZPE correction, turns out to be positive and around 0.4 eV. Likewise, the scattering calculations indicate the latter to be a bound state that move away from the continuum when a more accurate interaction is employed;
(ii) the next three metastable anions, all associated to excited electronic states of ($ANTH^-$), turn out to be well described by both CI(S) structural calculations and by the converged scattering calculations, both in positions on the energy scale and as three-dimensional wavefunctions mapping the spatial region of the molecular nuclei;
(iii) This special acene is therefore shown by our present calculations to constitute a specific example of condensed ring aromatic species: it represents, in fact, the smallest system beyond one- and two-ring acenes where correlation forces play an essential role in attaching into a physically bound state the extra-electron during the dynamical formation of the ANTH anion, ($ANTH^-$).

Acknowledgements

The financial support of the Italian PRIN2009 Research Network, project No.2009C28YBF-002 is gratefully acknowledged, as well as the computational support from the CINECA Consortium through its ISCRA Programme of research grants.

References

[1] S.P. Willner, B.T. Soifer, R.W. Russell, R.R. Joyce, F.C. Gillett, ApJ 217 (1977) L121.
[2] E. Peeters, S. Hony, C. van Kerckhoven, A.G.G.M. Tielens, L.J. Allamandola, D.M. Hudgins, C.W. Bouschlicher, A&A 390 (2002) 1089.
[3] W.A. Schutte, A.G.G.M. Tielens, L.J. Allamandola, ApJ 415 (1993) 397.
[4] J. Oomens, J.M. Bakker, B.G. Sartakov, G. Mejer, G. van Helden, Chem. Phys. Lett. 367 (2003) 576.
[5] D.K. Bohme, Chem. Rev. 92 (1992) 1487.
[6] D. Field, S.L. Lunt, S.V. Hoffmann, J.P. Ziesel, R.J. Gulley, in: V. Ossenkopf, J. Stutzki, G. Winnevisser (Eds.), The Physics and Chemistry of the Interstellar Medium, GCA-Verlag, Herdecke, 1999, p. 367.
[7] J.C. Rienstra-Kiracofe, C.J. Barden, S.T. Brown, H.F. Schaefer III, J. Phys. Chem. A 105 (2001) 524.
[8] S. Tobita, M. Meinke, E. Illenberger, L. Christophorou, H. Baumgartel, S. Leach, Chem. Phys. 161 (1992) 510.
[9] S. Lepp, A. Dalgarno, E.F. Van Dishoeck, J.H. Black, ApJ 329 (1988) 418.
[10] F. Carelli, F.A. Gianturco, Comp. Theor. Chem. 990 (2012) 67.
[11] F.A. Gianturco, R.R. Lucchese, J. Chem. Phys. 113 (2000) 10044.
[12] F. Carelli, M. Satta, F.A. Gianturco, Eur. Phys. J. D 67 (2013) 230.
[13] F. Carelli, T. Grassi, F.A. Gianturco, A&A 103 (2013) 549.
[14] P.D. Burrow, J.A. Michejda, K.D. Jordan, J. Chem. Phys. 86 (1987) 9.
[15] J. Schiedt, R. Weinkauf, Chem. Phys. Lett. 266 (1997) 201.
[16] N. Ando, M. Mitsui, A. Nakajima, J. Chem. Phys. 127 (2007) 201.
[17] A. Garcia-Sanz, F. Carelli, F. Sebastianelli, F.A. Gianturco, G. Garcia, New J. Phys. 15 (2013) 013018.
[18] J. Hachman, J.J. Darando, M. Avilès, G. Kin-Lac Chan, J. Chem. Phys. 127 (2007) 134309.
[19] B. Haigatò, D. Sziebert, P. Geerlings, F. De Proft, M.S. Deleuze, J. Chem. Phys. 131 (2009) 224321.
[20] R.R. Lucchese, F.A. Gianturco, Int. Rev. Phys. Chem. 15 (1996) 429.
[21] F.A. Gianturco, A. Jain, Phys. Rep. 143 (1986) 339.
[22] N. Sanna, F.A. Gianturco, R.R. Lucchese, J. Chem. Phys. 100 (1994) 6464.
[23] S.L. Altmann, H.P. Cracknell, Rev. Mod. Phys. 37 (1965) 19.
[24] S. Hara, J. Phys. Soc. Jpn. 22 (1967) 710.
[25] J.B. Foresman, M. Head-Gordon, J.A. Pople, M.J. Frisch, Phys. Chem. 96 (1992) 135.
[26] F.A. Gianturco, R.R. Lucchese, J. Chem. Phys. 108 (1998) 6144.
[27] J.P. Perdew, A. Zunger, Phys. Rev. B 23 (1981) 5048.
[28] N.T. Padial, D.W. Norcross, Phys. Rev. A 29 (1984) 1742.
[29] F.A. Gianturco, A. Jain, L.C. Pantano, J. Phys. B 20 (1987) 571.
[30] G.A. Gallup, J. Chem. Phys. 139 (2013) 104308.
[31] Online database, see http://astrochemistry.ca.astro.it/database/anthracene/anthracene.html
[32] M.A. Morreson, L.A. Collins, Phys. Rev. A 23 (1981) 127.
[33] R.R. Lucchese, V. McKoy, Phys. Rev. A 28 (1983) 1382.
[34] F.A. Gianturco, R.R. Lucchese, N. Sanna, A. Talamo, in: H. Ehrhardt, L.A. Morgan (Eds.), Electron Collisions with Atoms, Molecules, Clusters, Plenum, New York, 1994, p. 71.